Magnetic anisotropy, magnetization reversal and switching in Ni4Nb2O9 single crystals.

Magnetic anisotropy, magnetization reversal and switching in $Ni_4Nb_2O_9$ single crystals.

C. Martin[1], L. Hervé[1], D. Sedmidubsky[2], J.P. Bolletta[1,] F. Damay[3] and A. Maignan[1*]

[1] Laboratoire CRISMAT, Normandie Université, ENSICAEN, UNICAEN, CNRS, 14050 Caen, France.

[2] Department of Inorganic Chemistry, University of Chemistry and Technology Prague, Technicka 5, 166 28 Prague, Czech Republic

[3] Université Paris-Saclay, Laboratoire Léon Brillouin, CEA-CNRS UMR 12, 91191 GIF-SUR-YVETTE, France

* Corresponding author: antoine.maignan@ensicaen.fr

Abstract

$Ni_4Nb_2O_9$ is an insulating compensated ferrimagnet with T_N = 77 K and T_{comp} = 33 K. We report here the study of the magnetic anisotropy using millimeter-size crystals grown in an image furnace. The magnetization measurements, vs temperature, performed with *H* aligned along the three main crystallographic axes, show similar Curie-Weiss temperatures ($\Theta_p \approx$ 190K) and rather similar effective paramagnetic moments (from 3.5 μ_B to 3.6 μ_B). This suggests that the strongest magnetic interaction is the antiferromagnetic one, coupling the ferromagnetic distorted honeycomb layers and zigzag ribbons via face sharing NiO_6 octahedra. This strong antiferromagnetic coupling is supported by DFT calculations that do not evidence any inter site ferromagnetic interaction, leading to total compensation between magnetic moments of both Ni^{2+} sites. Measurements vs magnetic field below T_N reveal an anisotropic behavior, with square magnetization loops for *H* in the *ab* plane, whereas linear *M*(*H*) curves without hysteresis are observed for *H* // *c*. This anisotropy between *ab* plane and *c* axis occurs also in the magnetization reversal, which is observed in the *ab* plane only. Starting from *M*(*H*) virgin curves collected just below T_{comp}= 33K with *H* // *a* or *H* // *b*, the memory-like effect was tested through magnetization switching induced by *H* or *T* alternating changes. Below T_{comp}, smaller *H* is needed to switch *M* symmetrically for *H* along *b* than along *a*, and, for *T* switching (2 K interval, constant *H*), a larger *M* change is obtained along *a* than along *b*. The comparison with ferrimagnetic oxides which exhibit magnetization reversal, like spinels or rare earth orthoferrites, shows that $Ni_4Nb_2O_9$ is unique since only one magnetic cation over two sites in octahedral coordination is at play, thus providing a unique platform to study *M* switching but also a challenge for theoretical interpretation.

1. Introduction

Among the spintronics materials, ferrimagnets (FIM) are combining advantages of both ferromagnets (FM) with large enough magnetization to be detected or controlled by an external magnetic field and spin dynamics of antiferromagnets (AFM) faster than those of ferromagnets [1-4]. Ferrimagnets with large enough saturation magnetization, controllable magnetic anisotropy and large electrical resistivity are, for instance, used in high-density memories. In addition, some ferrimagnets -sometimes referred to as compensated FIM- undergo a magnetization reversal (MR) as the temperature decreases through their compensation temperature (T_{comp}) [5,6]. In the vicinity of this T_{comp}, the magnetization (M) can be switched from $M < 0$ to $M > 0$, by applying a magnetic field (H). Spinels are well known for showing this kind of behaviour, one example being Fe-substituted $Co(Cr_{1-x}Fe_x)_2O_4$ [7] where the MR is induced by the Fe substitution from x = 0.06 to x = 0.1. This illustrates the applicability of such materials in magnetic switching devices. Nevertheless, the rationalisation of the search for new compounds is not easy since negative magnetization may result from very different mechanisms [6] and since FIM occurs in different structures as spinels [1,7,8], perovskites [9-11], garnets [1] …. The common feature of all these compounds is that there is a site competition between several types of magnetic coupling, between two different cations occupying two different sites (as a transition metal and a lanthanide [11]) or between two sites occupied by the same element (as tetrahedra and octahedra in spinels [7,8]), which can also be influenced by disorder induced by substitution [7-11]. The competing magnetic interactions can also lead to interesting exchange bias and memory effects [7-11].

Among FIM with MR, polycrystalline samples of $Ni_4Nb_2O_9$, characterized by T_N = 77 K and T_{comp} = 33 K [12,13], have recently shown a reproducible M reversal induced by external magnetic field (H) or temperature (T) changes around T_{comp} [14]. Moreover, both T_N and T_{comp} have successfully been tuned by substituting Ni by either Co [15] or Zn [16]. The effect of substitution by Zn has also been studied theoretically to comprehend the phenomena underlying these changes [17]. $Ni_4Nb_2O_9$ offers thus a flexible platform for designing new FIM materials with MR, confirming the ever-renewed interest in nickel oxides in link with their often original behaviour in fields as varied as superconductivity, multiferroicity or oxygen diffusion [18-20].

Despite sharing the $A_4Nb_2O_9$ formula, $Ni_4Nb_2O_9$ does not crystallize in the $P\bar{3}c1$ corundum structure exhibited when A = Mn, Co or Fe [21] corresponding to AFM and linear magnetoelectrics [22-24]. Nevertheless, the $Ni_4Nb_2O_9$ structure drawn in Fig. 1 shows still similarities with corundum. It is described in the orthorhombic *Pbcn* space group with cell parameters a = 8.7688 Å, b = 5.0545 Å and c = 14.3041 Å [25]. The Ni^{2+} (S=1) cations, that occupy two crystallographic sites, and the Nb^{5+} ones, are all coordinated in O_6 octahedra linked by corners, edges or faces building *ab* layers stacked along the *c* axis.

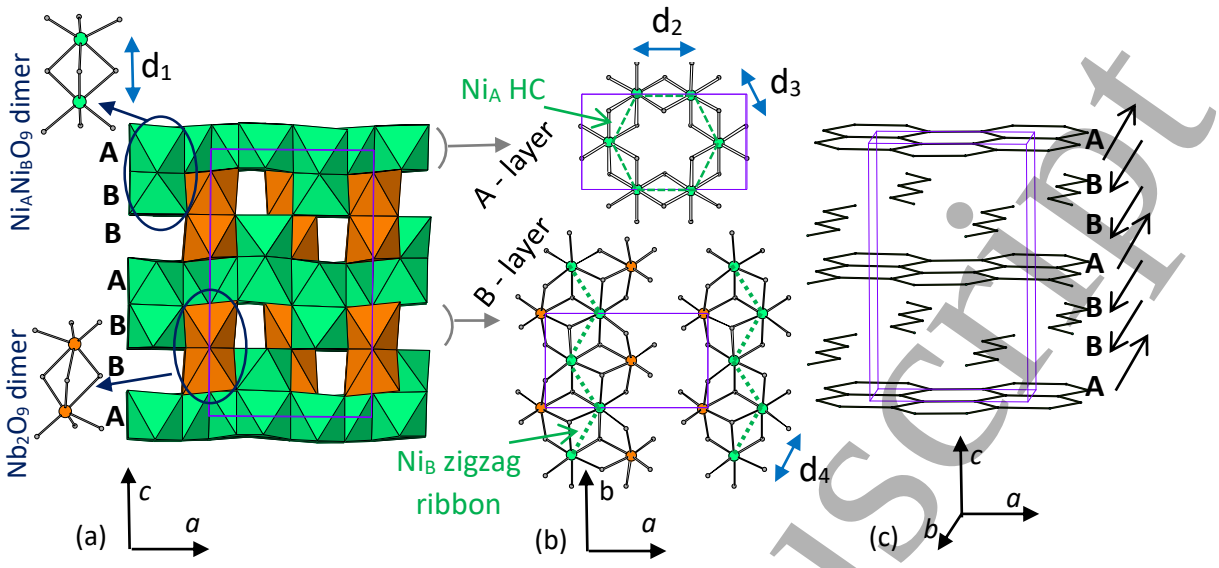

Figure 1. Drawings of the $Ni_4Nb_2O_9$ structure. (a) NiO_6 and NbO_6 octahedra are shown in green and orange, respectively. The ellipses indicate the Ni_2O_9 and Nb_2O_9 units, made of pairs of octahedra sharing a face, that are also presented on the left with the Nb-O and Ni-O bonds. (b) Projection along *c* of a Ni_A HC plane (top) and a B layer made of Ni_B zigzag ribbons (bottom). In (c) only the Ni sub lattice is drawn to highlight the HC and ribbons. The magnetic structure is symbolised by the arrows, the spins are all aligned along the *b* axis, the coupling is ferromagnetic in the ribbons and in the HC layer but antiferromagnetic between them. The main Ni-Ni distances are indicated $d_1 < d_2 < d_3 < d_4$.

Ni^{2+} cations describe a honeycomb-like (HC) framework in layer A, in which NiO_6 octahedra are sharing edges, with two close Ni-Ni distances ($d_2 < d_3$ in Fig. 1b top). In each B layer, one NiO_6 octahedron shares edges with two NiO_6 forming zigzag ribbons running along *b* (with a Ni-Ni distance $d_4 > d_3$ in Fig. 1b bottom). Each NiO_6 has also common edges with three NbO_6 octahedra. The connection between A and B layers corresponds to pairs of Ni_AO_6 and Ni_BO_6 octahedra sharing a face and thus to the shortest Ni-Ni distance (d_1 in Fig. 1a). Nb_2O_9 dimers ensure the connection between two successive B layers (Fig. 1a). The magnetic structure consists of FM A and BB layers, that are AFM coupled along *c*. This AFM coupling corresponds to the shortest Ni-Ni distance in the material ($d_1 \approx 2.66$ Å). The number of Ni^{2+} is the same in both A and BB layers, and the octahedral distortion is large for both sites but slightly larger for Ni_BO_6 as discussed later. The main difference concerns the topology of both layers (HC and zigzag ribbon for A and B, respectively) and thus the magnetic exchange pathways. Ni_A and Ni_B magnetic moments are similar, as proved by neutron powder diffraction studies, which also showed that the magnetic moments are aligned along the *b* axis [13], as illustrated in Fig. 1c. Collinear spins, together with the layered structure of the compound, suggest a strong anisotropy in the magnetic properties, that could also influence the magnetization reversal in $Ni_4Nb_2O_9$. For this reason, it was appealing to grow crystals of $Ni_4Nb_2O_9$ to study the magnetic properties along the three crystallographic axis and clarify the extent of its anisotropic magnetic behaviour.

2. Materials and methods

2.1 Sample preparation

Well sintered polycrystalline rods of $Ni_4Nb_2O_9$ (≈ 6 mm diameter and several cm long) were prepared starting from 30 g of a stoichiometric mixture of 4 NiO + 1 Nb_2O_5. The powders were first heated in air at 900°C (during two days) before being crushed again and sieved to 250 μm. They were then introduced into flexible latex tubes (of diameter 6 mm) to be pressed at 3000 bars in a medium made of 75% mineral hydraulic oil and 25% white spirit. The so-obtained cylinders of compacted powder were then heated in air up to 1300°C during 30 h. This synthesis process is derived from the one previously used for the production of bars [15]. To assess the quality of the rods, a small portion was crushed and then checked by means of X-ray powder diffraction (XRPD) using a Panalytical diffractometer equipped with a Cu source. The diffractograms were characteristic of the expected phase.

Crystal growth was then performed by the floating zone method, using a Crystal System Corporation image furnace (FZ-T-10000-H-III-P) with four mirrors and four 500 W halogen lamps. The growth was stabilized at 83.2% of the power of the lamps, under 8.5 bar of oxygen pressure. The as-prepared rods, used as feeding and seeding parts, were rotated in opposite directions at 20 rpm. The displacement of the molten zone was ensured by the translation of the mirrors at 2.75 mm/hour. Over one day, a crystal of ≈ 6 mm diameter with a length of ≈ 6 cm was obtained.

A small part of crystal was ground for XRPD, confirming the $Ni_4Nb_2O_9$ compound was obtained. Several pieces were cut according to desired orientations for magnetic characterizations using a Laue Crystal Orientation System (Photonic Science) and the OrientExpress software [26].

2.2 Magnetic characterization

Magnetic moments (*m*) were recorded in magnetic fields (*H*) using a 5.5x10^4G SQUID magnetometer from Quantum Design. The magnetization (*M*) was calculated as $M = m/mass$ and the magnetic susceptibility as $\chi = M/H$.

The magnetic properties were characterized using platelets of mm size, with the magnetic field aligned along *a*, *b* or *c*, and using several pieces. Indeed, the measurements were performed along the three crystallographic axes of one sample but also using several samples to probe the reproducibility of results and also to discard any size or shape effects. The measurements along each crystallographic axis yield similar magnetization values for samples with short (< 1mm) or long (> 5mm) dimensions

along this direction. In practice, the crystals were mounted on straws and attached using tape. The alignment error is estimated to be less than 5° in every case.

As far as MR is concerned, the experimental process has to be carefully controlled to avoid effects due to different cooling histories related to temperature sweeping and remnant magnetic fields. In particular, a demagnetization sequence (Demag) for the superconducting magnet of the magnetometer leaving a remnant magnetic field of +1.0 G was systematically used in between series of measurements. To do so, the field set first at $-3x10^4$ G was returned to 0 by using the "Oscillate mode". After that, measurements of the remnant magnetic field of the coil using a paramagnetic sample allowed to confirm a reproducible +1.0 G value. Thus, in addition to temperature stabilization of the crystal at 150 K, i.e. 70 K above T_N, to erase the magnetic history of the sample, Demag was performed to ensure to always start from the same experimental conditions, i.e. an external magnetic field of +1.0 G and a temperature of 150 K.

The temperature dependence of M was measured in warming in zero-field-cooling (zfc) and field-cooling (fc) modes. The sample was first cooled down to 5 K, temperature at which H = 100 G was applied before measuring versus temperature in settle mode up to 300 K (zfc). Then, the sample was cooled in the same magnetic field down to 5 K and finally measurements taken upon warming (fc). Also, a field-cooling curve in -100 G was also collected for one orientation with measurements taken upon warming.

Complete hysteresis loops ($M(H)$) were also collected at 10 K and 50 K, i.e. below and above the compensation temperature (T_{comp}= 33 K), respectively. For each one, after Demag, the sample was cooled to 5 K before heating up to the collection temperature.

The magnetization "switching" from $M < 0$ to $M > 0$, first evidenced in polycrystalline samples [14], was then performed along the three crystallographic axes, using two types of experiments. First, magnetization switching induced by magnetic field was measured at 32K, by alternating H from H_1 to H_2. The determination of the H_1 to H_2 values for each orientation was made thanks to a $M(H)$ curve collected at 32 K from 0 to 5000 G by 100 G step. Second, the temperature induced magnetization reversal was tested at 100 G, by varying temperature from T_1 = 32 K to T_2 = 34 K, with measurements performed by sweeping at 0.5 $K.min^{-1}$ to collect points in the transition between the two states.

2.3 DFT calculations

The electronic structure calculations were performed within VASP 5.4 program as implemented in MedeA 3.6 software package using a Projector Augmented Waves method (PAW) [27] and a Generalized Gradient Approximation (GGA) with PBE parametrization scheme [28] combined with an

additional effective on-site Coulomb potential U_{eff} = U–J = 3.5 eV laid on the Ni-*3d* states [29]. The integration was performed using a tetrahedron method with Blöchl corrections on a mesh of k-points within the first Brillouin zone with a density 0.25 Å^{-1}.

3. Results

3.1 Magnetic measurements, electronic structure calculations and anisotropy

From the zfc and fc $M(T)$ curves recorded with the magnetic field aligned along the principal directions of the crystals (Fig. 2a), the ferrimagnetic transition is observed at the same T_N = 77 K value as for polycrystalline samples. Nonetheless, these zfc and fc $M(T)$ curves evidence strong differences. When H is aligned along the c axis, the magnetic behaviour differs strongly from the $M(T)$ curves recorded for H aligned along a or b as no negative magnetization is observed and far below T_N the M values are smaller by a factor of 10. In contrast, the $M(T)$ curves recorded for H aligned along a or b evidence M < 0 values at low temperature for both zfc and fc curves, with a crossing of the zfc and fc curves corresponding to M = 0 at T_{comp} = 33 K. The shape of the curves is rather similar for both configurations but larger M absolute values (positive and negative) and smaller differences between zfc and fc curves are obtained for $H \parallel a$ than for $H \parallel b$. The field-cooling curve collected in -100 G for $H \parallel a$ (inset of Fig. 2a) is perfectly symmetric with the fc in 100 G. These observations show that c is the hard axis and ab the easy plane, in agreement with the magnetic structure established by neutron powder diffraction [13].

In the paramagnetic regime, the fitting of the linear part of the inverse susceptibility curves between 200 K and 300 K with $\chi^{-1} = (T + \Theta_p)/C$ gives an excellent matching (Fig. 2b). Adding a constant χ_0 term was not found to improve the fit quality for the 200 K - 300 K range. From the Curie constant C, similar μ_{eff} values per Ni are extracted for the three directions, 3.50 μ_B, 3.53 μ_B and 3.62 μ_B for H along a , b and c, respectively, i.e. very close to the value reported for polycrystalline samples, μ_{eff} = 3.66 μ_B [13], that is higher than expected for the S = 1 spin only value (μ_{eff} = 2.89 μ_B). The higher μ_{eff} suggest the only partial extinction of the orbital moment. Consequently, the spin-orbit coupling inducing a lifting of the orbital degeneracy, it can be responsible for a strong temperature dependence of the local magnetic moments [30]. This might explain why the $\chi^{-1}(T)$ curve fitting over larger temperature range, even by including a constant term, was not as good as over the high temperature only. Thus, one has to be cautious when interpreting the obtained parameters.

The three similar Θ_p values (192 K, 187 K and 195 K, for H along a, b and c, respectively) suggest that the same main AF exchange mechanism is dominating in the paramagnetic state for the three directions. The main difference between easy plane and hard axis is the departure from linearity occurring below 200 K (the lower temperature of the range used for the fitting). This upward deviation

on the χ^{-1} (*T*) curves being at higher temperature for *H* parallel to *a* or *b* than to *c* suggests stronger antiferromagnetic fluctuations in plane.

For the three orientations, the magnetization *M(H)* loops recorded at 10 K and 50 K (Fig. 3), i.e. below and above T_{comp}, confirm the conclusions drawn from the *M(T)* curves and are consistent with ferrimagnetism. The *M*(*H*) curves recorded with *H* along *a* or *b* have similar shapes at 10 and 50 K (Fig. 3a and b). The hysteresis loops at 50 K exhibit smaller coercive field (H_c) and larger remnant magnetization (M_{rem}) values than at 10 K. The highest M_{rem} value, 0.083 μ_B/f.u. corresponding to 0.021 μ_B/Ni, is reached when *H* is aligned along *a*. This is a much lower value than the complete ferromagnetic alignment of the S=1 Ni^{2+} magnetic moment, which would correspond to 2μ_B, supporting the only small difference $|m_{NiA}-m_{NiB}|$ evidenced in the refined magnetic moments (2.0 and 1.7 μ_B, respectively) [13].

The antiferromagnetic coupling occurring between ferromagnetic layers of almost identical m_{NiA} and m_{NiB} is supported by the DFT band structure calculations that revealed a pure antiferromagnetic ground state with the same magnitude of spin-up (S = 0.83) and spin-down (S = -0.83). The antiferromagnetic ground state was found to be stabilized by 8.8 kJ/mol f.u. with respect to the ferromagnetic arrangement. The inclusion of spin-orbit (S-O) did not change any essential features of the electronic structure and indicated a negligible orbital moment (≈ 0.2 μ_B). Nevertheless, the S-O calculation with the selected magnetization axis along *b* yielded a ground state slightly stabilized by 8 J/mole f. u. (2 J/ mole Ni) compared to the other two orientations of the magnetization axis, *a* and *c* (being surprisingly equal in energy).

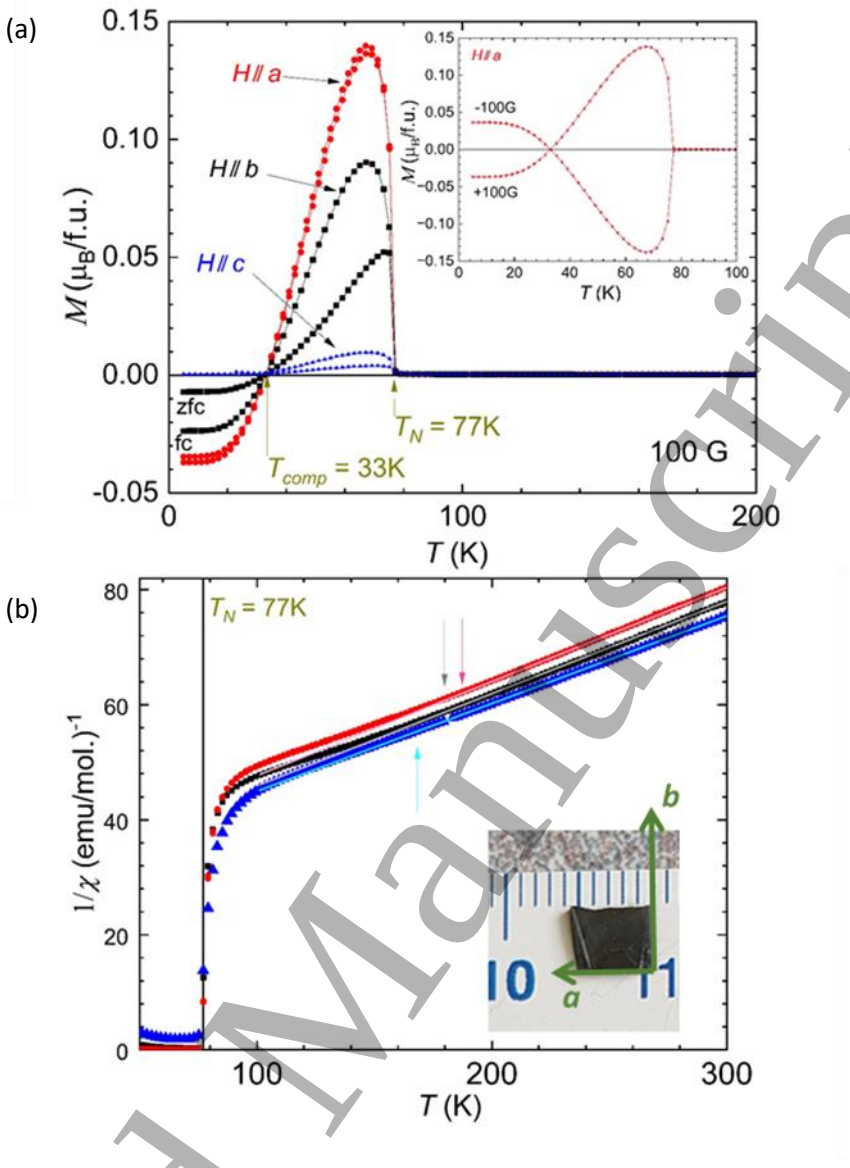

Figure 2. (a) Magnetization curves vs temperature with *H* aligned along *a*, *b* or *c* axis. The magnetic ordering temperature T_N and the compensation temperature T_{comp} are indicated by vertical arrows. zfc and fc labels, for zero field cooling and field cooling within 100 G, are given for the *H // b* configuration since it shows the larger difference between the two curves. In inset, fc curves collected in +100 and -100 G with *H // a*. (b) inverse magnetic susceptibility curves, with same colour and symbols code, superimposed pink, grey and cyan lines are for the fits of the $\chi^{-1}(T)$ curves in their linear part (between 200 and 300K) *;* vertical arrows indicate approximatively the departure from linearity. The piece of crystal used for these measurements is also shown.

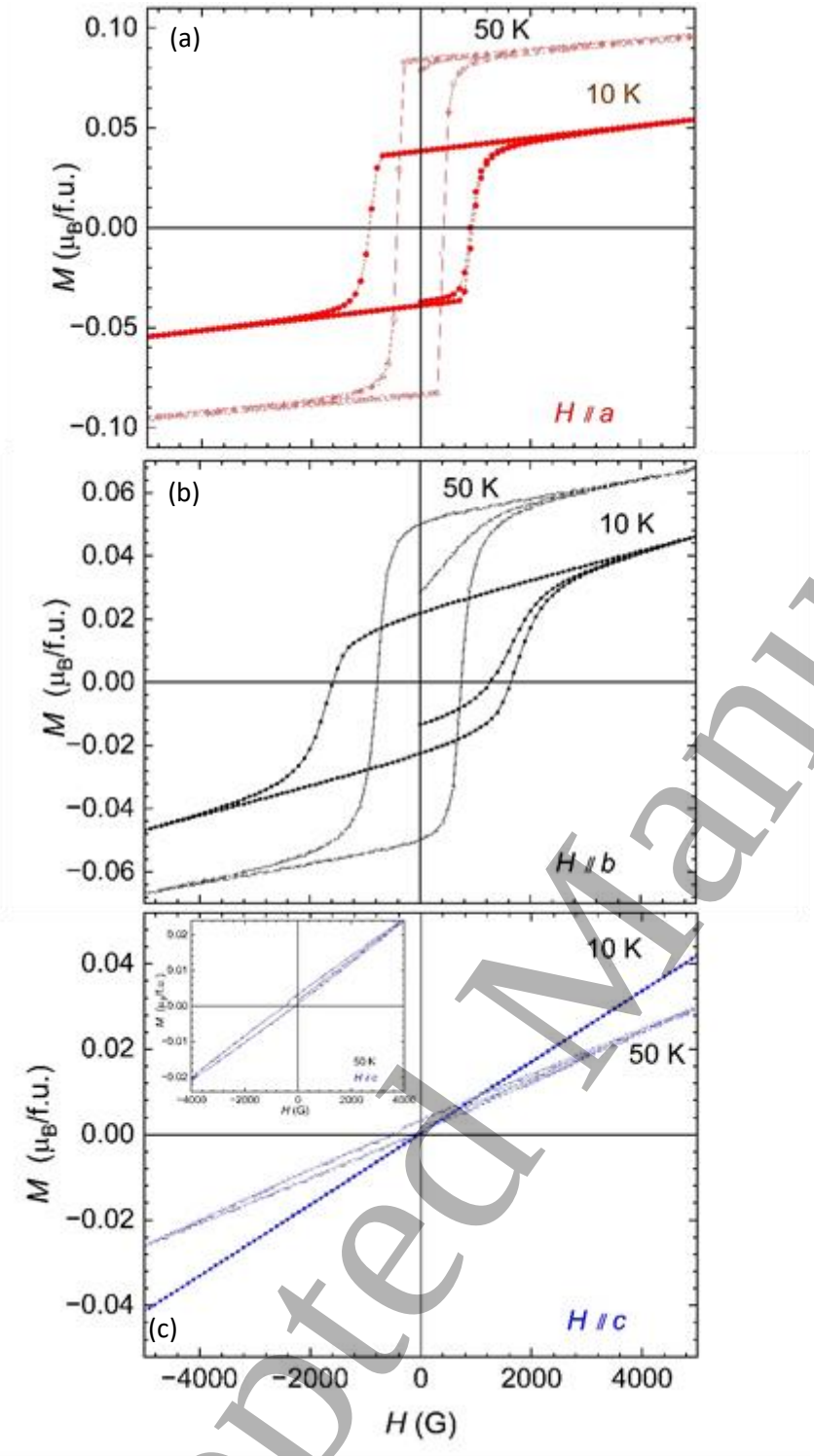

Figure 3. Magnetization *M(H)* loops recorded at 10 K and 50 K for *H* along *a*, *b* or *c*. The *y*-axis of the 50 K loop of Fig. 3c is expanded in inset to show the (*x*,*y*) off-centring attributed to exchange bias.

The density of states shows a broad valence band (from -6 eV up to the Fermi level) of predominantly O-2*p* character with a strong admixture of Nb-4*d* and Ni-3*d* states. The band gap for the spin-down channel is narrower by ≈ 0.75 eV due to higher energy of valence band maximum contributed by Ni_B-3*d* states and the conduction band minimum with the predominant Ni_A-*3d* character. Moreover, an asymmetry in the density of states for the spin-up and spin-down channel is clearly seen at the band gap maximum and minimum (Fig. 4a) indicating a different crystal field effect on the respective Ni sites, in agreement with the different distortions of the Ni_AO_6 and Ni_BO_6 octahedra. It is highlighted in Fig. 4b where the twelve Ni-O distances of a $Ni_ANi_BO_9$ dimer are reported, the characteristic parameters for each Ni are given on the right and the average of the four sets of three Ni-O distances is indicated on the left. Apart from the larger Ni_B-O distance variance, the rotation angle between the $O_{3\text{-out}}$ and $O_{3\text{-in}}$ triangles is shifted by ≈ 7° from an ideal antiprismatic coordination in Ni_BO_6, while it remains nearly ideal (60°) in the case of Ni_AO_6. Hence, although both Ni_A and Ni_B site symmetries can be roughly approximated by C_3 point group (the real symmetry being C_1), Ni_B experiences a more distorted octahedral field. It should be noted that DFT, even within the GGA-U functional, cannot account for the combined effect of crystal field distortion and S-O coupling, which is likely at the origin of the enhanced magnetic anisotropy and the preferred spin orientation. At the same time, the admixture of the excited localized states of ^3A and ^3E symmetry into ^3A ground state (considering C_3 symmetry) via S-O coupling might result in zero-field splitting (ZFS) and, consequently, in a slightly lower magnetic moment on Ni_B site (due to higher coordination distortion) and the observed ferrimagnetic behaviour [13].

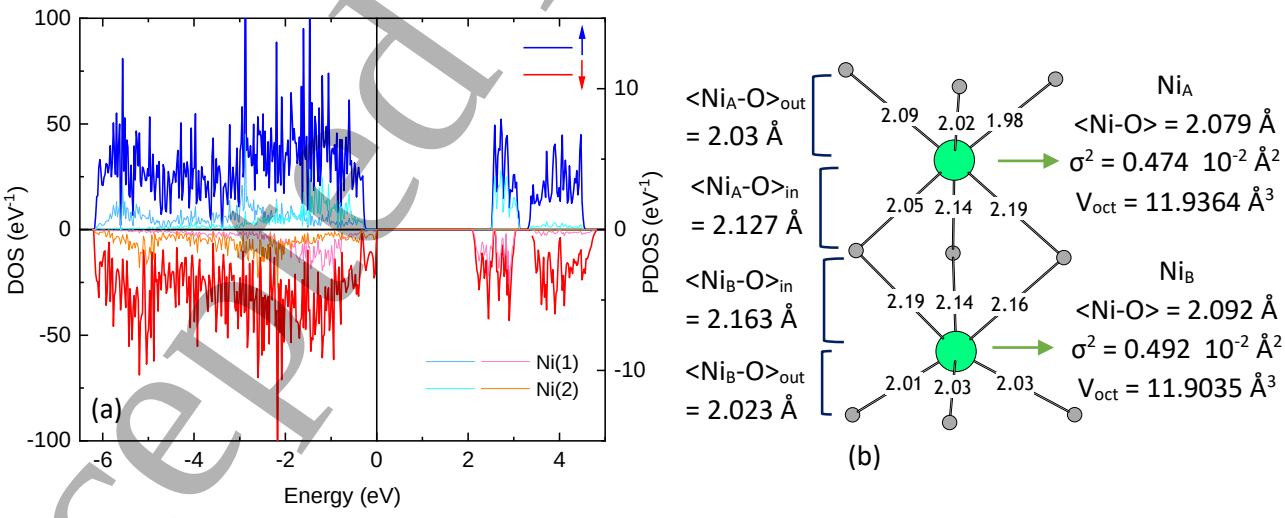

Figure 4. (a) Density of states (DOS) and site projected partial DOS (PDOS) versus energy of $Ni_4Nb_2O_9$ calculated by MedeA-VASP (GGA+U, U= 3.5 eV) for spin up and spin down channel assuming an antiferromagnetic arrangement of Ni_A and Ni_B. (b) Distortion of the two types of NiO_6 octahedra forming a dimer (from synchrotron XRPD at 15 K [13]), the Ni-O distances are indicated. For each Ni, the average Ni-O distance, their variance and the volume of the O_6 octahedra are given on the right. On the left, the average of each set of three distances is also given.

The behaviour for *H* along *c* (Fig. 3c) differs from the *ab* plane one, with a linear *M*(*H*) dependence at 10 K consistent with the antiferromagnetic coupling along this axis [13]. Furthermore, though a very small hysteresis loop is observed at 50 K, the loop is off centred (inset of Fig. 3c), which is characteristic of atomic exchange bias. The report of exchange bias in several compensated ferrimagnetic transition metal oxides supports this hypothesis, like in polycrystalline samples of $CoCr_2O_4$ spinel [7,8] or in so-called rare-earth ferrimagnets like orthorhombic perovskites, such as single crystals of $NdMn_{0.8}Fe_{0.2}O_3$ [9], $ErFeO_3$ and $GdCrO_3$ [10], and $SmFeO_3$ [11]. Though additional measurements are necessary to go further, as done for crystals of $ErFeO_3$ orthoferrite [31], the competing antiferro- and ferro-magnetic interactions in $Ni_4Nb_2O_9$ crystal are supposed to produce exchange bias as in other compensated ferrimagnets [7-11].

3.2 Magnetization reversal

As first reported for a $Ni_4Nb_2O_9$ polycrystalline sample by Meng et al [14], in the (*H,T*) region near T_{comp} where $M < 0$, *M* can be reversed reversibly from $M < 0$ to $M > 0$ by changing either *H* or *T*. In the isothermal case, the *M* sign change, indicating that the magnetic domains can reverse their magnetization, creates a "memory-like" with two *M+ and M-* states. To test a possible *M* reversal along each of the three crystallographic axes, isothermal *M*(*H*) first magnetization curves were recorded at 32 K, which is 1 K below T_{comp}, allowing a first comparison to be made with results presented in ref. [14]. The three $M(H)_{32K}$, collected from 0 to 5000 G in steps of 100 G (Fig. 5) are linear starting from $M < 0$ at $H = 0$ for $H \parallel a$ and *b*, with *M* absolute value three times larger in the *a* case. By increasing *H*, these curves show that *M* can be switched to $M > 0$ in both cases. In contrast, the $M > 0$ values of the $M(H)_{32K}$ along the *c* axis are not compatible with MR. As illustrated for measurements at T_{comp}=33K along *a* or *b*, the $M(H)_{33K}$ curves show $M = 0$ at $H = 0$, indicating that the material behaves like an antiferromagnet at T_{comp}, where it is precisely balanced. For each direction the $M(H)_{33K}$ and $M(H)_{32K}$ are parallel. These measurements justify the choice of 32K and 34K to reverse magnetization by temperature.

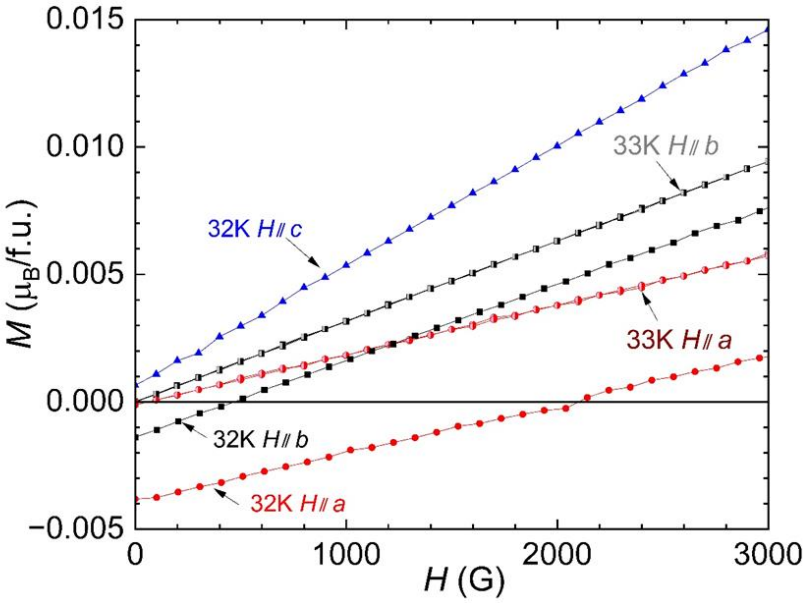

Figure 5. *M(H)* magnetization curves collected at 32 K, with *H* aligned along *a*, *b* or *c*. Data were also collected at 33 K for *H* along *a* and *b*.

Considering that the $M(H)_{32K}$ slope increases from *a* to *b*, a larger magnetic field is requested to reach $M = 0$ for *H* parallel to *a*, i.e. 2110 G against 450 G for *H* aligned to *b*. These values allow to select *H* values to control the *M* reversal from $M < 0$ to $M > 0$ at 32 K. Indeed, if rather symmetric *M* "switching" ($M_+ \approx -M_-$) can be obtained by varying *H* between 100 G and 1000 G for *H* along *b* (Fig. 6b), larger *H* values are required along *a,* to reverse *M*, as for instance between 200 G and 3000 G (Fig. 6a). This is highlighted by the curves in the middle part of Fig. 6b (32 K, 200 G and 3000 G) showing that similar *H* values do not produce $|M+|$ *and* $|M-|$ equal values for *H* // *b*.

In the same way, a difference is also observed in *T*-induced *M* reversal along *a* and *b*. Keeping 100 G for both orientations, and by varying *T* between 32K and 34K, which correspond to +/-1 K around T_{comp}, *M* changes sign for both *a* and *b* with larger *M* absolute values for the *a* direction (Fig. 6a and 6b). With this technique of magnetic moment measurement, the dynamics of the *T* induced *M* reversal cannot be probed, and more adapted technique like laser pulses would be needed [2].

To summarize, for *H*-induced *M* reversal at 32 K, i.e. 1 K below T_{comp}, smaller *H* values are necessary to reverse *M* for *H* along *b* than along *a*. For *T*-induced reversal within a 2 K interval and at same *H*, a larger *M* change is obtained along *a* than along *b*. This can be connected to the *M*(*T*) too, as the *H* // *a* curve has a steeper slope when crossing T_{comp}. This could be possibly used as a predictor in other MR materials.

4. Discussion and concluding remarks

The study of $Ni_4Nb_2O_9$ single crystals reveals the anisotropy of the magnetization below the magnetic ordering temperature (T_N = 77 K). In particular, when *H* is applied along *c*, magnetization reversal is not observed, whereas along either *a* or *b*, the reversal is observed below T_{comp} (= 33 K) for small *H*. This demonstrates the magnetization reversal anisotropy of $Ni_4Nb_2O_9$, in agreement with its magnetic

structure [13] described by the antiferromagnetic coupling along *c* of ferromagnetic *ab* planes. Nevertheless, the *M(T)* curves (Fig. 2a) collected with *H* along *a* and *b* suggest that *a* is the easy-axis, whereas smaller *H* values are necessary to reverse *M* for *H* along *b* than *a* direction. This difference supports a weak in-plane anisotropy. In addition, angular measurements with *H* rotating in the *ab* plane would be necessary to determine unambiguously the easy axis.

To our knowledge, $Ni_4Nb_2O_9$ is the only compound with this structure that combines honeycomb layers and zigzag chains of NiO_6 octahedra stacked along *c*. Its originality also concerns the type of FIM that occurs, since more often it deals with non collinear magnetic structures, several magnetic cations (or at least unbalanced cation distribution) and several coordination polyhedra (as tetrahedra and octahedra in spinels) [6]. A difference of distortion implies a difference of crystal field, which implies a difference of ordered magnetic moment, thus favors FIM, as already proposed in the $Ni_{4-x}Zn_xNb_2O_9$ series with the report of quadratic elongation of the octahedral vs *x* [17]. The larger distortion of the Ni_BO_6 octahedra is also visible in Fig. 4b with a larger value of the variance and a smaller "out" and larger "in" <Ni-O> for Ni_B than Ni_A. This is undoubtedly linked to the fact that NbO_6 polyhedra are linked more strongly with Ni_BO_6 than Ni_AO_6, i.e. by edges and apexes, respectively. In addition, the difference in the neighboring, with 2 next neighbors (NN) in the ribbon and 3 in the HC layer, has probably to be taken into account too. Indeed, in $NiNb_2O_6$ that crystallizes in the columbite structure, the NiO_6 octahedra also form zigzag files in which the arrangement of the moments is FM (*FxCz)* [32]. On the other side, Ni_3TeO_6, from corundum type, is described as a collinear AFM with FM HC planes [33]. The magnetic couplings observed in $Ni_4Nb_2O_9$ are thus coherent with those reported for Ni_3TeO_6 and $NiNb_2O_6$.

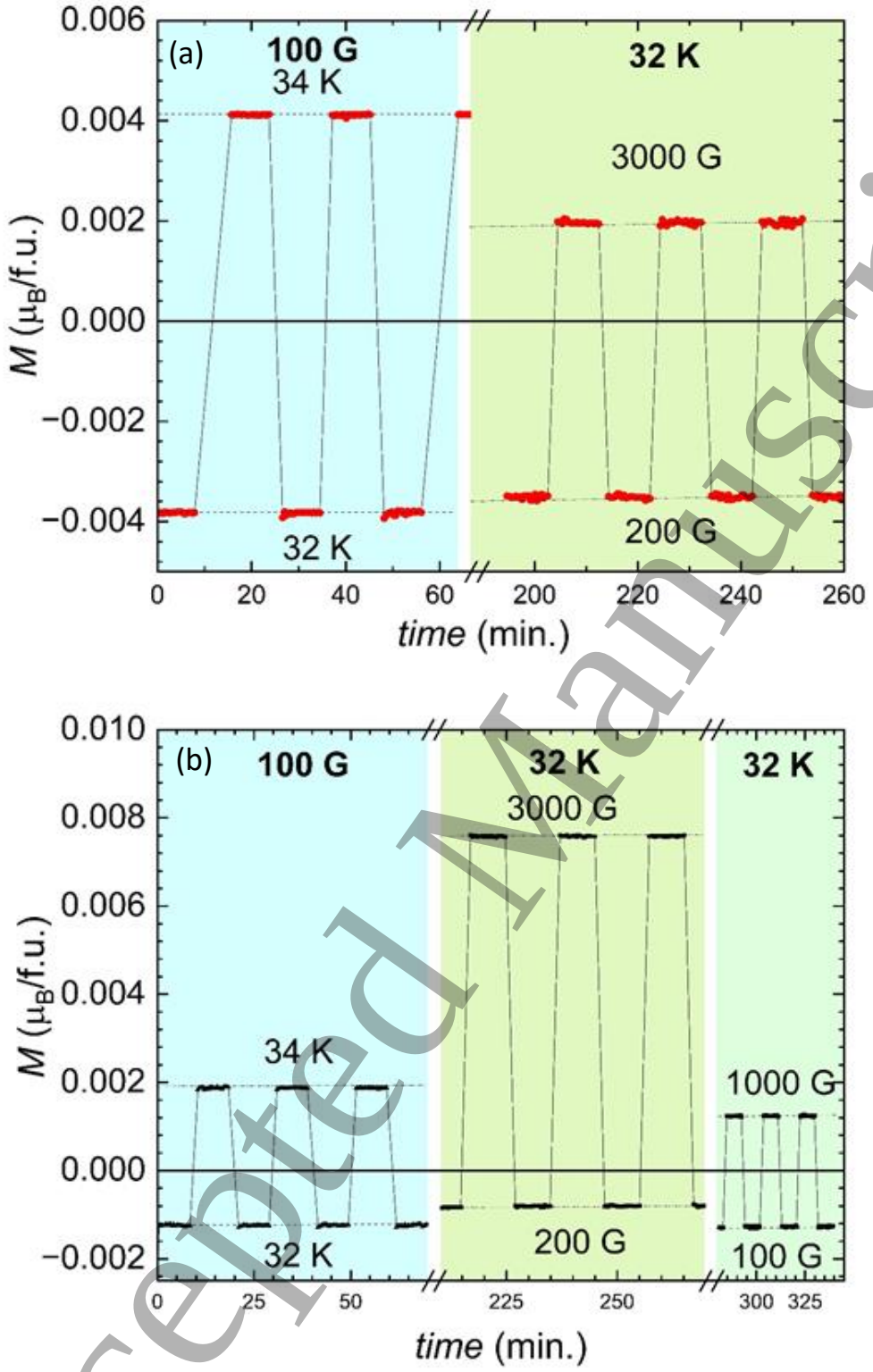

Figure 6. Magnetization reversal induced by temperature (MR) or by magnetic field with *H* // *a* (a) and // *b* (b).

In agreement with its peculiar magnetic ground state, $Ni_4Nb_2O_9$ exhibits unexpected characteristics, as (i) the same value of T_{comp} whatever H applied along a or b, that is in contrast with the observations made on $NdMn_{0.8}Fe_{0.2}O_3$ single crystals, a ferrimagnet showing also magnetization reversal [9] and (ii) similar values of Θ_p along the three directions, that clearly differ from $Ni_2Mo_3O_8$, an antiferromagnet where Ni cations form also a honeycomb lattice [19]. Nevertheless, surprisingly, it seems that the conditions for observing magnetization reversal vs H in the vicinity of T_{comp} in $Ni_4Nb_2O_9$ are of the same order of magnitude as in other systems. Among ferrimagnetic oxides that exhibit magnetization reversal, substituted $CoCr_2O_4$ [7,8] showing also H-induced M switching, requires H values alternating between 50 G and 2000 G, at 2K below T_{comp}, i.e. for T and H values very close to those of the switching in $Ni_4Nb_2O_9$ crystals.

As perspective, the realization in $Ni_4Nb_2O_9$ of -1 and +1 magnetization states under H of 100 G and 1000 G (Fig. 6b) could be used to design volatile memory since when H = 0, M returns to the negative state [6]. Moreover, the MR through T_{comp} might be exploited for thermo-magnetic switches. However, since there is no report for M reversal induced by alternating T in other compounds like $CoCr_2O_4$ [7,8], a comparison is still to be done. In the context of magnetic memory, the present crystals offer also opportunities to test the existence of exchange bias in a new type of FIM oxides.

Finally, as Zn for Ni substitution in polycrystalline samples was shown to be efficient in reinforcing the MR with $|M|$ and T_{comp} increasing with the Zn content, crystals of $(Ni,Zn)_4Nb_2O_9$ would be worth growing.

Acknowledgment: JPB, AM and CM acknowledge the financial support of the French Agence Nationale de la Recherche LabEx EMC3 through the Project MaPhoOBi (Grant No. ANR-10-LABX-0009), and the Normandy Region (Réseau d'Intérêt Normand - Label d'excellence).

References

1. S. Emori and P. Li, Ferrimagnetic insulators for spintronics: Beyond garnets, J. Appl. Phys. 129, 020901 (2021).
2. M. V. Logunov, S. S. Safonov, A. S. Fedorov, A. A. Danilova, N. V. Moiseev, A. R. Safin, S. A. Nikitov, and A. Kirilyuk, Domain Wall Motion Across Magnetic and Spin Compensation Points in Magnetic Garnets, Phys. Rev. Appl. 15, 064024 (2021).
3. S. K. Kim, G. S. D. Beach, K.-J. Lee, T. Ono, T. Rasing, and H. Yang, Ferrimagnetic spintronics, Nat. Mater. 21, 24 (2022).
4. Y. Zhang, X. Feng, Z. Zheng, Z. Zhang, K. Lin, X. Sun, G. Wang, J. Wang, J. Wei, P. Vallobra, Y. He, Z. Wang, L. Chen, K. Zhang, Y. Xu, and W. Zhao, Ferrimagnets for spintronic devices: From materials to applications, Appl. Phys. Rev. 10, 011301 (2023).
5. L. Néel, Propriétés magnétiques des ferrites; ferrimagnétisme et antiferromagnétisme, Ann. Phys. Paris 12, 137 (1948).
6. A. Kumar and S. M. Yusuf, The phenomenon of negative magnetization and its implications, Phys. Rep. 556, 1 (2015).
7. C.L. Li, T.Y. Yan, G.O. Barasa, Y.H. Li, R. Zhang, Q.S. Fu, X.H. Chen, S.L. Yuan, Negative magnetization and exchange bias effect in Fe-doped $CoCr_2O_4$, Ceramics International 44, 15446 (2018).
8. R. Padam, Swati Pandya, S. Ravi, S. Ramakrishnan, A.K. Nigam, A. K. Grover and D. Pal, J. Study of the sign change of exchange bias across the spin reorientation transition in $Co(Cr_{1-x}Fe_x)_2O_4$ (x = 0.00–0.125), J. Phys.: Condens. Matter 29, 055803 (2017).
9. M. Mihalik Jr., J. Pospíšil, M. Mihalik, Magnetization reversal in $NdMn_{0.8}Fe_{0.2}O_3$ single crystal, Journal of Magnetism and Magnetic Materials 541, 168531 (2022).
10. E.E. Zubov, Crystal field and origin of exchange bias in compensated rare-earth ferrimagnets, Journal of Magnetism and Magnetic Materials 551, 169153 (2022).
11. X.-X. Wang, S. Gao, X. Yan, Q. Li, J.-C. Zhang, Y.-Z. Long, K.-Q. Ruand and X.-G. Li, Giant spontaneous exchange bias obtained by tuning magnetic compensation in samarium ferrite single crystals, Phys. Chem. Chem. Phys. 20, 3687 (2018).
12. H. Ehrenberg, G. Wltschek, H. Weitzel, F. Trouw, J. H. Buettner, T. Kroener, and H. Fuess, Ferrimagnetism in $Ni_4Nb_2O_9$, Phys. Rev. B 52, 9595-9600 (1995).
13. E. Tailleur, C. Martin, F. Damay, F. Fauth, and A. Maignan, Lack of linear magnetoelectric effect in ferrimagnetic distorted honeycomb $Ni_4Nb_2O_9$, J. Appl. Phys. 127, 063902 (2020).
14. B. Meng, X. T. Ji, X. H. Chen, Q. S. Fu, C. L. Li, C. Chakrabarti, Y. Qiu, and S. L. Yuan, Negative magnetization effect in distorted honeycomb $Ni_4Nb_2O_9$ ceramics, J. Low Temp. Phys. 207, 115-126 (2022).
15. J. N. Jiongo-Dongmo, J. P. Bolletta, A. Maignan, F. Damay and C. Martin, The $Ni_{4-x}Co_xNb_2O_9$ phase diagram: from magnetization reversal to linear magnetoelectricity, J. Mater. Chem. C 11, 5092-5101 (2023).
16. J. P. Bolletta, F. Fauth, C. Martin, and A. Maignan, Magnetization reversal tuning in honeycomb ferrimagnet $Ni_4Nb_2O_9$, J. Appl. Phys. 132, 153901 (2022).
17. E. Rufeil Fiori, J. P. Bolletta, C. Martin, A. Maignan and O. V. Billoni, Magnetization reversal study of $Ni_{4-x}Zn_xNb_2O_9$ compounds using Monte Carlo simulations, J. Phys.: Condens. Matter 36, 015801 (2024).
18. M. R. Norman, Entering the nickel age of superconductivity, Physics 13, 85 (2020).
19. P. Yadav, S. Lee, G. L. Pascut, J. Kim, M. J. Gutmann, X. Xu, B. Gao, S.-W. Cheong, V. Kiryukhin, and S. Choi, Noncollinear magnetic order, in-plane anisotropy, and magnetoelectric coupling

in the pyroelectric honeycomb antiferromagnet $Ni_2Mo_3O_8$, Physical Review Research 5, 033099 (2023).

20. S. R. Maity, M. Ceretti, R. de Barros, L. Keller, J. Schefer, A. Cervellino, J.A.Rodriguez Valamazan , and W. Paulus, Large-scale oxygen order phase transitions and fast ordering kinetics at moderate temperatures in Nd_2NiO_{4+d} electrodes, Mater. Adv. 4, 651 (2023).
21. E. F. Bertaut, L. Corliss, F. Forrat, R. Aleonard, and R. Pauthenet, Etude de niobates et tantalates de métaux de transition bivalents, J. Phys. Chem. Solids. 21, 234-251 (1961).
22. Y. Fang, W. P. Zhou, S. M. Yan, R. Bai, Z. H. Qian, Q. Y. Xu, D. H. Wang, and Y. W. Du, J. of Magnetic-field-induced dielectric anomaly and electric polarization in $Mn_4Nb_2O_9$, Appl. Phys. 117, 17B712 (2015).
23. Y. Fang, Y. Q. Song, W. P. Zhou, R. Zhao, R. J. Tang, H. Yang, L. Y. Lv, S. G. Yang, D. H. Wang, and Y. W. Du, Large magnetoelectric coupling in $Co_4Nb_2O_9$, Sci. Rep., 4, 3860 (2014).
24. A. Maignan and C. Martin, $Fe_4Nb_2O_9$: a magnetoelectric antiferromagnet, Phys. Rev. B 97, 161106 (R) (2018).
25. R. Wichmann, and H. Müller-Buschbaum, Eine neue kristallstruktur des nickel-oxoniobats: II-$Ni_4Nb_2O_9$, Z. Anorg. Allg. Chem. 539, 203-210 (1986).
26. B. Ouladdiaf, J. Archer, G.J. McIntyre, A.W. Hewat, D. Brau, and S. York, OrientExpress: A new system for Laue neutron diffraction, Phys. B: Condens. Matter 385-386, 1052-1054 (2006).
27. G. Kresse, and D. Joubert, From ultrasoft pseudopotentials to the projector augmented-wave method, Phys. Rev. B 59 [3] 1758 (1999).
28. J.P. Perdew, K. Burke, and M. Ernzerhof, Generalized gradient approximation made simple, Phys. Rev. Lett. 77 [18] 3865-3868 (1996).
29. L. Dudarev, S.Y. Savrasov, C.J. Humphreys, and A.P. Sutton, Electron-energy-loss spectra and the structural stability of nickel oxide: an LSDA+U Study, Phys. Rev. B 57 [3] 1505-1509 (1998).
30. M. W. Haverkort, A. Tanaka, Z. Hu, H. H. Hsieh, H.-J. Lin, C. T. Chen, and L. H. Tjeng, Low energy excitations in CoO studied by temperature dependent x-ray absorption spectroscopy, ArXiv:0806.3736. (2008)
31. I. Fita, A. Wisniewski, R. Puzniak, V. Markovich, and G. Gorodetsky, Exchange-bias reversal in magnetically compensated $ErFeO_3$ single crystal, Phys. Rev. B 93, 184432 (2016).
32. C. Heid, H. Weitzel, F. Bourdarot, R. Calemczuk, T. Vogt, and H. Fuess, Magnetism in $FeNb_2O_6$ and $NiNb_2O_6$, J. Phys.: Condens. Matter 8, 10609 (1996).
33. I. Zivkovic, K. Prsa, O. Zaharko, and H. Berger, Ni_3TeO_6-a collinear antiferromagnet with ferromagnetic honeycomb planes, J. Phys.: Condens. Matter 22, 056002 (2010).